

Automated Segmentation of 7 Tesla MRI

By Lisa Karstens Vingara, PhD

A Capstone

Presented to the Department of Medical Informatics and Clinical Epidemiology
and the Oregon Health & Science University
School of Medicine
in partial fulfillment of
the requirements for the degree of
Master of Biomedical Informatics
September 2013

School of Medicine
Oregon Health & Science University

CERTIFICATE OF APPROVAL

This is to certify that the Master's Capstone Project of

Lisa K. Vingara

"Automated Segmentation of 7 Tesla MRI"

Has been approved

Eilis Boudreau, MD, PhD

TABLE OF CONTENTS

List of Figures and Tables.....	4
Acknowledgments.....	5
Part 1: Introduction to Magnetic Resonance Imaging and Challenges at Ultra High Magnetic Fields.....	6
1.1 Basic Introduction to Magnetic Resonance Imaging.....	7
1.2 Magnetic Field Strength.....	11
1.3 Automatic Segmentation of the Brain.....	12
Part 2: Automated Segmentation at 7 Tesla.....	15
2.1 Introduction.....	16
2.2 Bias Field Correction.....	16
2.3 Brain Extraction.....	20
2.4 Tissue Segmentation.....	21
2.5 Comparison of Methods on 7T Data.....	22
2.6 Discussion.....	34
References.....	37

LIST OF FIGURES

Figure 1: MRI	9
Figure 2: T ₂ and T ₁ weighted images.....	10
Figure 3: 3T vs. 7T.....	12
Figure 4: Bias field inhomogeneity at 7T.....	17
Figure 5: Bias field correction	19
Figure 6: Brain extraction	21
Figure 7: FSL FAST segmentation.....	25
Figure 8: Impaired image alignment SPM.....	25
Figure 9: Overview of grey matter segmentation methods.....	27
Figure 10: Overview of white matter segmentation methods.....	28
Figure 11: Overview of CSF matter segmentation methods.....	29
Figure 12: Color overlays different segmentation methods.....	30
Figure 13: Scatter plots of segmentation results.....	31
Figure 14: Segmentation versus age.....	33

LIST OF TABLES

Table 1: Tissue volumetrics.....	26
----------------------------------	----

ACKNOWLEDGEMENTS

I would like to thank my academic advisor, Dr. Eilis A. Boudreau, and research mentor, Dr. William D. Rooney for their support and guidance on this capstone project as well as throughout my time at OHSU. I have had a wonderful experience working with William Rooney's lab learning about structural MR image processing and in vivo phosphorous spectroscopic imaging at ultra high magnetic fields. I am very fortunate to have had the opportunity to work with both of them and I am extremely grateful for their encouragement and guidance through the beginning of my academic career. I would also like to thank all of the students, faculty and staff members within the bioinformatics program, as well as those at the Advanced Imaging Research Center at OHSU for being such wonderful people to work with. I would especially like to thank Yosef, Manoj, and Brendan for their extensive help learning MRI and computational techniques used in image analysis.



Part 1

**Introduction to Magnetic Resonance Imaging and Challenges at
Ultra High Magnetic Fields**

The focus of this project was to evaluate automatic segmentation routines on magnetic resonance images acquired at 7 Tesla. The first part of this capstone introduces the basic concepts of Magnetic Resonance Imaging (MRI) and ultra high magnetic fields. The second part focuses on specific automated segmentation methods and their application to ultra high field MRI data.

1.1 Basic Introduction to Magnetic Resonance Imaging

Magnetic resonance imaging (MRI) allows for the non-invasive exploration of animal and human anatomy. MRI was first formally introduced by Paul Lauterbur in 1973, whereby applying position dependent magnetic fields (gradients) in addition to a static magnetic field, a number of different one-dimensional profiles were obtained of the water content in glass capillary tubes.^[1] Using procedures similar to those developed for computer tomographic X-ray scanning, these profiles were then combined in order to reconstruct the two-dimensional image.^[2] In the early 1980's, MRI was introduced into the clinical setting and is now in mainstream clinical use for noninvasively diagnosing anatomical ailments and is used extensively in research to understand the pathophysiology of disease.

Modern imaging utilizes gradients for frequency encoding, phase encoding, and slice selection in the x, y, and z directions, respectively. By adding a gradient to the static \mathbf{B}_0 magnetic field, slice selection isolates a single plane in the object being imaged. This imposes a gradient of the nuclei-specific Larmor frequency along the z-axis and only spins in this plane will be excited when the radio frequency (RF) pulse is applied. Frequency encoding generates a spectrum of spin distribution along the x-axis, while phase encoding causes a phase offset proportional to the spin's position along the y-axis.^[3] This provides the two-dimensional spatial information for the

selected slice, which when Fourier transformed gives rise to an image of spin location and density.

Due to its large natural and biological abundance, hydrogen is mostly used for imaging. The human body is primarily fat and water, both of which contain a large number of hydrogen molecules, making approximately 63% of the human body hydrogen.^[4] The nuclear magnetic resonance signal is characterized by two principal relaxation properties; i) the longitudinal time constant, T_1 , which describes the time scale needed to polarize the nuclear spin system and establish equilibrium magnetization along the axis parallel (longitudinal) to the external magnetic field (\mathbf{B}_0), and ii) the transverse relaxation time constant, or T_2 , which describes the timescale of an NMR phase coherence transverse to the static magnetic field established by a radiofrequency pulse. The hydrogen molecules will have different relaxation times depending on the structure of the tissue's environment. Figure 1 shows a representative MRI in which different structures of the brain can be distinguished due to these properties. The presence of larger molecules, such as proteins and fat, will cause water protons in tissues high in these constituents to have short nuclear magnetic resonance relaxation time constants. For compartments with low macromolecular content, such as cerebrospinal fluid (CSF) spaces, water protons have much longer relaxation time constants. Additional contrast mechanisms can be used exploiting the T_1 and T_2 relaxation parameters for various human tissues.

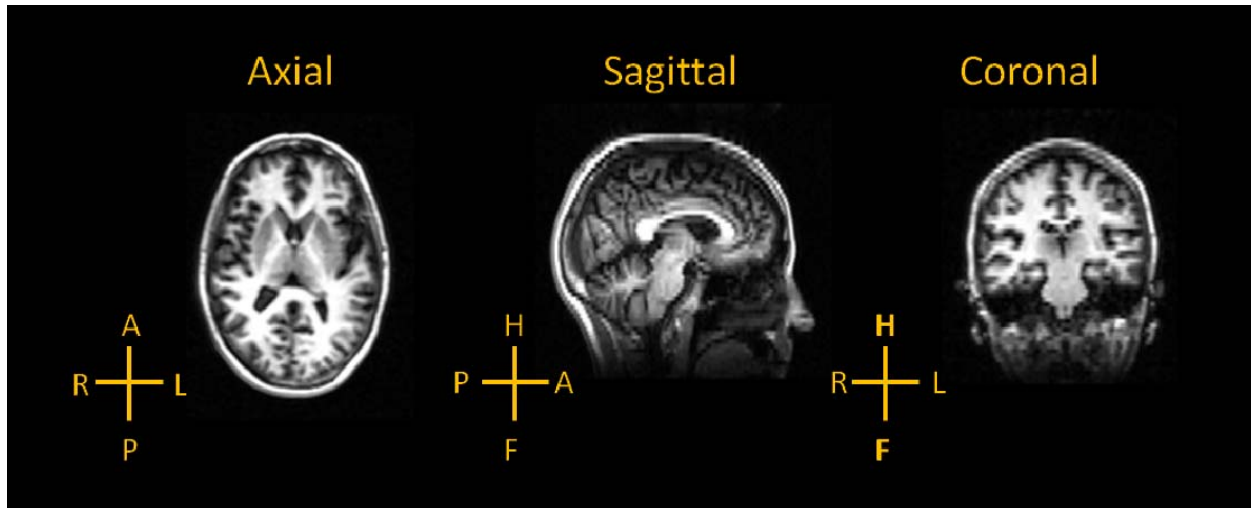


Figure 1. From left to right: axial, sagittal, and coronal T_1 weighted MRI of a healthy individual's head at 3T. The different contrast of tissues is primarily due to differences in T_1 relaxation of the hydrogen atoms in the tissues. White matter, which has a short T_1 , is bright, while grey matter is darker than white matter, and CSF, with an even longer T_1 than grey matter is the darkest. A- Anterior; P- Posterior; R- Right; L-Left; H- Head; F- Foot.

In order to enhance contrast of particular features, different properties of tissue can be exploited. T_1 weighted images are used to give preferential saturation of faster relaxing protons, such as protons located in white matter. These protons will show up brighter on the image than longer relaxing protons, such as those contained in the CSF. This is done by the use of short echo times (TE) and short repetition times (TR). T_2 weighted images, on the other hand, use a spin echo technique with long TE and long TR, causing the strength of the signal to depend on the T_2 relaxation that occurs during the TE such that CSF will show up brighter than white matter (Figure 2).

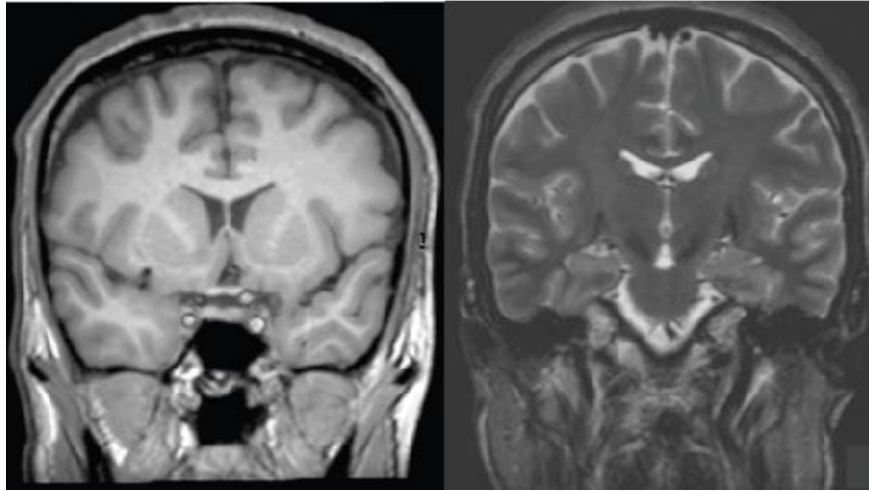


Figure 2. A coronal T₁ weighted MRI (left) and T₂ weighted MRI (right) of a healthy individual. The CSF in the ventricles is dark on the T₁ weighted image and bright on the T₂ weighted image, whereas white matter is light on the T₁ weighted image and dark on the T₂ weighted image. This is due to the different relaxation properties that the pulse sequences take advantage of.

In addition to T₁ or T₂ weighted imaging, contrast agents can be used to change the relaxation properties, and hence contrast, between tissues. Paramagnetic contrast agents promote spin-lattice and spin-spin relaxation of water molecules by creating time varying magnetic fields with both the rotational motion and electron spin flips associated with the unpaired electrons in the contrast agent.^[4] Gadolinium (Gd³⁺) chelated compounds are the most commonly used contrast agents, due to the seven unpaired electrons on Gd³⁺, which promotes very efficient spin relaxation due to flipping spins and rotational motion.^[4]

Structural MRI allows for examination of the brain non-invasively. Brain tumors typically appear as abnormalities that are readily visible on MRI, and certain tumors can be distinguished from each other based on their appearance on a MRI. In other neurological disorders, such as multiple sclerosis, white matter hyperintensities are readily identifiable and can assist in diagnoses of specific disorders. In research settings, MRI is commonly used in order

to better understand how the brain changes with and during the disease. It is also of interest to determine if there are structural changes either globally or regionally in disease states.

1.2 Magnetic Field Strength

MRI instruments have a strong magnetic field that is used to align the magnetization of the atomic nuclei, typically hydrogen, in the body. The standard magnetic field strength in a clinical setting is 1.5T, though 3T scanners are also approved for clinical use. In research settings, 3T and 4T magnets are very common and allow for higher resolution images or shorter scan times when compared to lower field MRI. Since the signal to noise ratio increases with increasing magnetic field strength, a large effort has been made to develop stronger magnets.

Recently, technology has advanced and ultra high field magnets at 7T, 8T, and 9.4T are now available. These MRI systems are currently only approved for research purposes, but are showing great promise for future clinical applications. The signal to noise ratio continues to increase linearly with a 1.6 increase in signal to noise ratio from 4T to 7T.^[9] This increase in signal to noise is especially beneficial for functional MRI (fMRI), susceptibility-weighted imaging, and spectroscopy. High-resolution anatomical MR images can also be obtained at these field strengths with an isotropic resolution as low as 0.5 mm allowing to view finer anatomical structure than previously available.^[10] Due to the inherent trade-off between scan time and signal, imaging at higher magnetic fields can also be used to shorten scan time, making some imaging techniques more clinically feasible.

While there are many benefits to imaging at ultra high magnetic fields, there are also technical limitations and disadvantages. Artifacts are non-trivial at ultra high magnetic fields such as 7T since the length of the radiofrequency waves in tissue will be on the order of

centimeters rather than meters as at 1.5T.^[9] This shorter wavelength is now in the range of organs in the body and leads to artifacts (Figure 3), which lead to technical difficulties in acquiring and processing the data. Vaughan et al. calculated the variation in the \mathbf{B}_1 magnetic field to be nearly twofold higher in 7T images compared to 4T images.^[9]

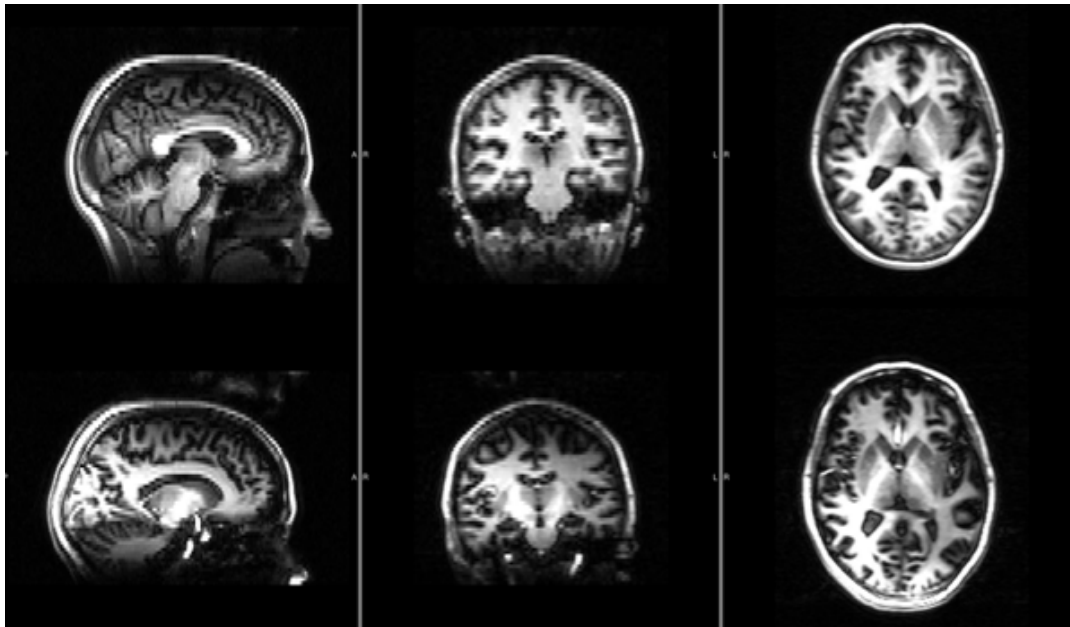


Figure 3. MRI from the same participant at 3T (top panel) and 7T (lower panel). Despite the higher resolution, the intensity varies greatly in the 7T images. This is due to the inhomogeneity of the \mathbf{B}_1 field. Also note the drop off in signal toward the neck, which is more extreme in the 7T image than the 3T image.

1.3 Automatic Segmentation of the Brain

Three-dimensional segmentation of the brain includes measuring cerebral tissues such as white matter, grey matter, cerebrospinal fluid, in addition to specific cerebral structures such as the thalamus or hippocampus, from the three-dimensional volumes called voxels that make up the MRI. Manual segmentation involves tracing the borders of the tissue or structure of interest

by hand and is time consuming, difficult, costly, and subjective. With the advances in imaging, where high resolution images can be collected with hundreds of slices per dimension, this task quickly becomes infeasible. Automated segmentation is highly desirable for this task and can make tissue segmentation time efficient, practical, and consistent across users.

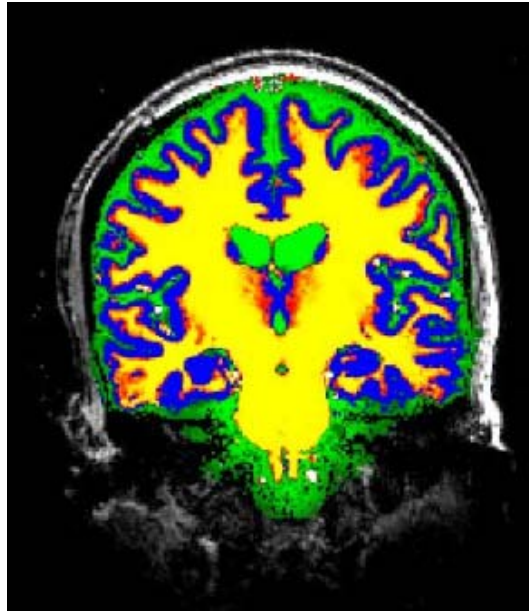
Aside from quantifying the amount of tissues in a person's brain, segmenting the image into different tissue classes (white matter, grey matter, cerebrospinal fluid, and lesions) is a common preprocessing step in more advanced analyses such as measuring cortical thickness or measuring regional grey matter atrophy with voxel-based morphometry. All of these measures are important for exploring the changes in cerebral volume and morphology in neurological diseases as well as in normal and abnormal aging.

Many techniques for automated and semi-automated tissue segmentation exist in the literature, are based on a wide range of principles, and vary in the degree of manual interaction. There are methods that are based on thresholding,^[11] clustering,^[12] histograms,^[13] artificial neural networks,^[14] or hidden markov models,^[15] just to name a few. Desirable qualities of a segmentation routine are that it be fast, robust, and mostly automated.

While there are many different techniques for image segmentation, there are only a few widely used programs that implement a handful of these techniques: FMRIB Software Library (FSL, FMRIB, Oxford, UK.), Statistical Parametric Mapping (SPM8, Wellcome Trust Centre for Neuroimaging, London, UK.) and Freesurfer (Athinoula A. Martinos Center for Biomedical Imaging, Charlestown, Massachusetts). These programs are all open source, with readily available code that can be customized by the user. Additionally, they are well supported by the community as well as developers. Other programs do exist, but they are typically not well

supported, not open source which makes them difficult to alter and understand, do not have user extensive communities, and lack developer support. While FSL, SPM8, and Freesurfer are commonly used for segmentation and other MRI analysis, they were optimized for MRI at 1.5T or 3T, and may not function well for data collected at 7T, which has different challenges than lower field data, such as intensity variation across the image due to magnetic field inhomogeneities.

While the end goal is tissue segmentation of the MR images, there are many necessary processing steps that must be achieved for the segmentation to be successfully carried out. These are: bias field correction, brain extraction, and image registration. We will evaluate how FSL and SPM8 perform these tasks on 7T image data.



Part 2

Automated Segmentation at 7 Tesla

2.1 Introduction

Automated processing and segmentation of 7T MRI data using two software packages were compared: SPM8 and FSL. SPM8 is a software package that implements a variety of methods used in the analysis of functional and structural neuroimages. While SPM8 is freely available, it is implemented in Matlab and requires a Matlab license. SPM8 is primarily meant to be used with the graphical user interface (GUI), though there are some tools available through NiPype^[16] to automate the processes. FSL is a software library of tools for MR image analysis and is freely available. FSL is command line based and runs on Linux. It has both a GUI and command line interface, which allows for interactive or automated processing. In addition to evaluating the tools available in these two packages, the processing and segmentation analysis from Berlow et al.^[17] was also used as a comparison and is referred to as Berlow's method. Berlow's method used a variety of customized FSL tools and R1 maps to perform quantitative segmentation 7T MRI data.^[17]

2.2 Bias Field Correction

One major problem for automated tissue segmentation is the signal intensity variation across the brain volume caused by inhomogeneity of the B_1 field, referred to as the bias field. At ultra high magnetic fields such as 7T, this intensity variation is much worse than at lower fields (Figure 4). This inhomogeneity causes problems for automatic processing algorithms since homogenous signal and contrast are essential prerequisites for accurate processing of images. While there is a bias field present in images acquired at 1.5T and 3T, the variation induced across the field are much more subtle than at 7T and can be adjusted for by algorithms available in most automatic segmentation packages.

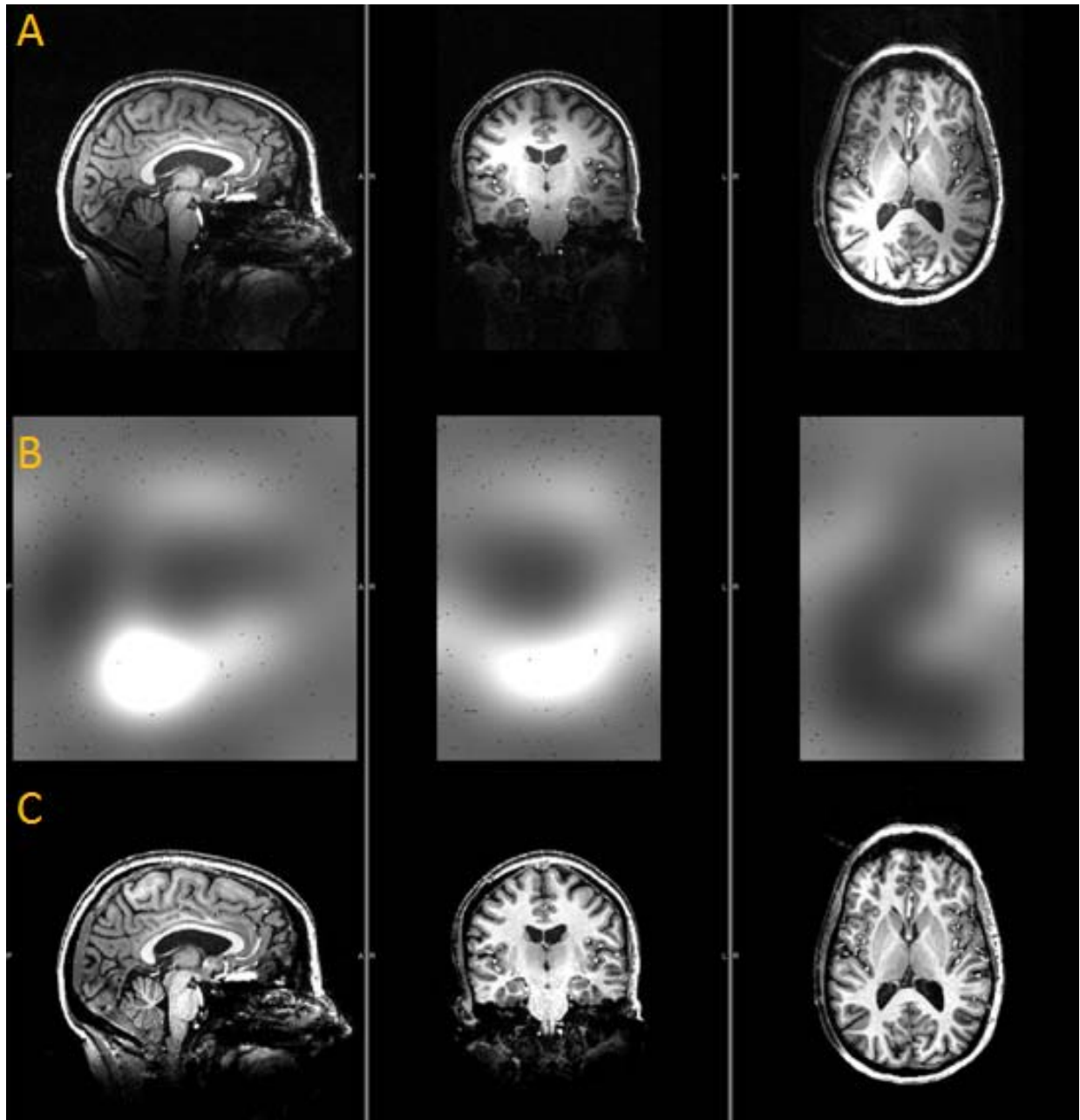


Figure 4. An example of the bias field inhomogeneity at 7T. (A) An MRI collected at 7T. The intensity of the image varies across the image. (B) The corresponding bias field correction needed to correct the bias field (C).

However, processing the 7T images with these algorithms optimized for 1.5T and 3T images usually leads to a poor correction of the bias field, which then influences subsequent processing steps and analyses. FSL's FMRIB's Automated Segmentation Tool (FAST) program for tissue segmentation incorporates bias field correction. The bias field is modeled as multiplicative and is iteratively adjusted for during the segmentation process.^[15] The automatic bias field correction in FSL is not effective at correcting the bias field in 7T MPRAGE images (Figure 5b).

To correct the bias field in 7T images, Berlow et al. initially estimated the bias field using a 3D Gaussian smoothing kernel (sigma 10 mm).^[17] The original image was then divided by the estimated bias field and normalized by the mean intensity of the original image. This method was additionally applied to the tissue masks of grey and white matter. This results in excellent correction of the bias field inhomogeneities (Figure 5C).

In SPM8, to correct the non-uniformity caused by the bias field, a Bayesian model is used to estimate a smooth function that is multiplied with the image using prior knowledge about the field distributions likely to be encountered.^[18] The assumed model for the inhomogeneity of the field is that the noise is multiplicative and due to variations of the tissue properties in each voxel, rather than due to noise from the scanner. To alter the bias field correction in SPM8, the user can change the full-width-half-maximum (FWHM) of the Gaussian smoothness of bias. For smoother intensities of the bias field, larger FWHM should be used. The default of very light bias regularization of 0.0001 gave satisfactory results for the majority of 7T images (Figure 5D).

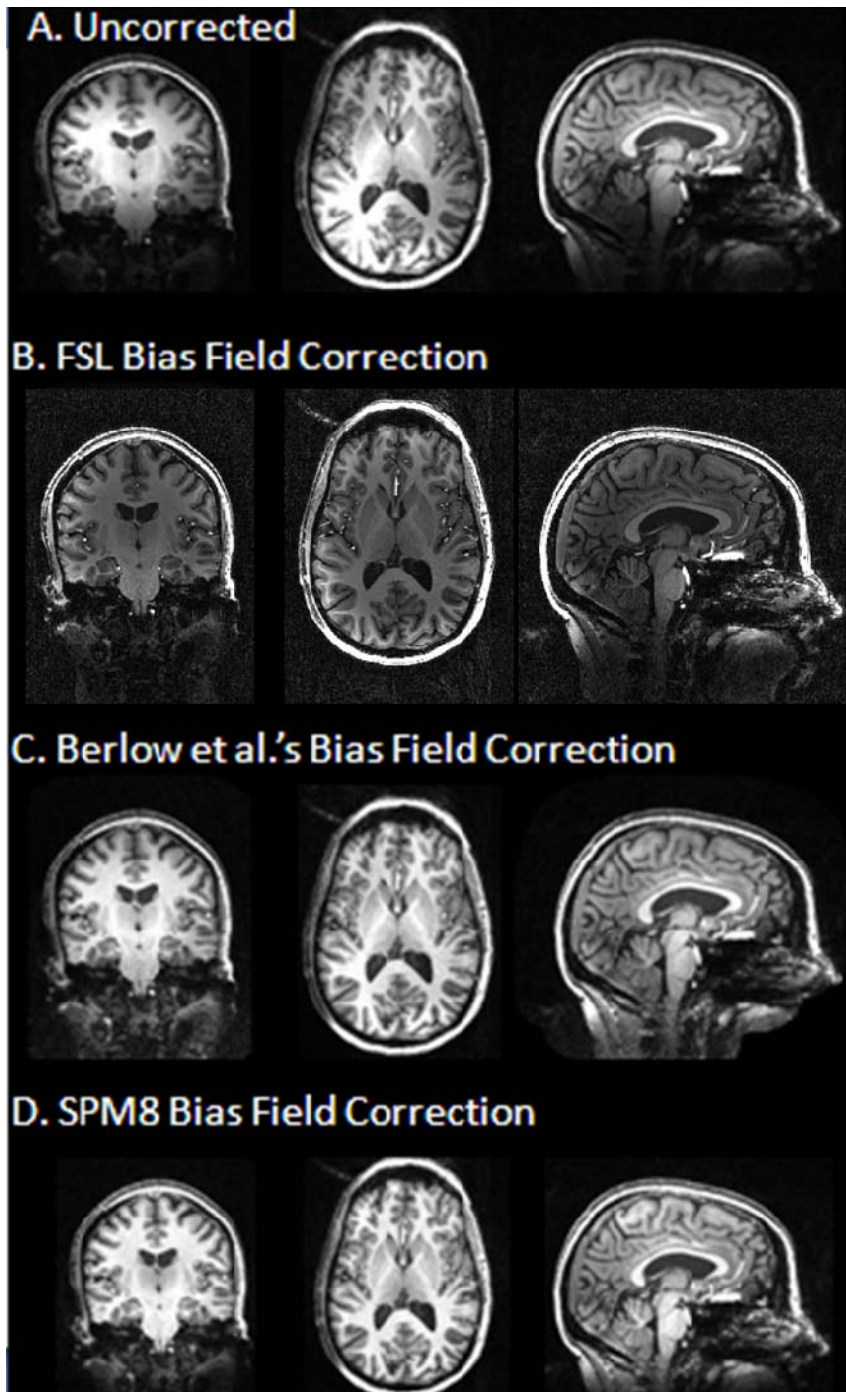


Figure 5. Methods for bias field correction applied to 7T MR images. (A) An uncorrected 7T high resolution MPRAGE MRI. Notice the brightness of the intensity in the lower left hand corner of the middle image in A that becomes dark in the lower right and upper left of the image. (B) FSL's bias correction performs poorly on these images, evident by the existence of the non-uniform intensity variation and poor tissue contrast after correction. (C) Berlow's method using preprocessing steps to estimate and correct the bias field. (D) SPM8's iterative bias correction performs well on the 7T data with default parameters.

2.3 Brain Extraction

Since the brain is the organ of interest, it is ideal to remove all other surrounding structures before segmenting the brain into tissue classes. This includes removal of all non-brain tissue such as the skull, scalp, eyes, sinus cavities, and muscle which may be misclassified if they remain in the image. FSL requires that the brain extraction is done prior to segmentation with FSL's Brain Extraction Tool (BET). Since it is a separate program, BET is highly flexible and there are many options that can be altered to attain good brain extraction.

In SPM8, the brain extraction is performed with the segmentation and is therefore not as flexible as FSL's BET. In the New Segmentation tool in SPM8, three additional templates are included to model non-brain tissue in addition to white matter, grey matter, and CSF. This indirectly performs the brain extraction.

While the FSL BET program is highly flexible, it yields poor results with 7T data. The neck and eyes are commonly in the resulting brain images, and the brain edges are sharp and rugged rather than smooth, even after tweaking the many of the parameters. Additionally, BET typically excludes parts of the brain close to the skull (Figure 6A), and parts of the brain stem and cerebellum on 7T images. While the SPM8 brain extraction is included in the segmentation step and is not easily altered, the algorithm and default settings in SPM8 work well with 7T images. There are a few voxels in the background that are incorrectly labeled as brain tissue, as shown in Figure 6B. These background voxels could be removed by masking the image.

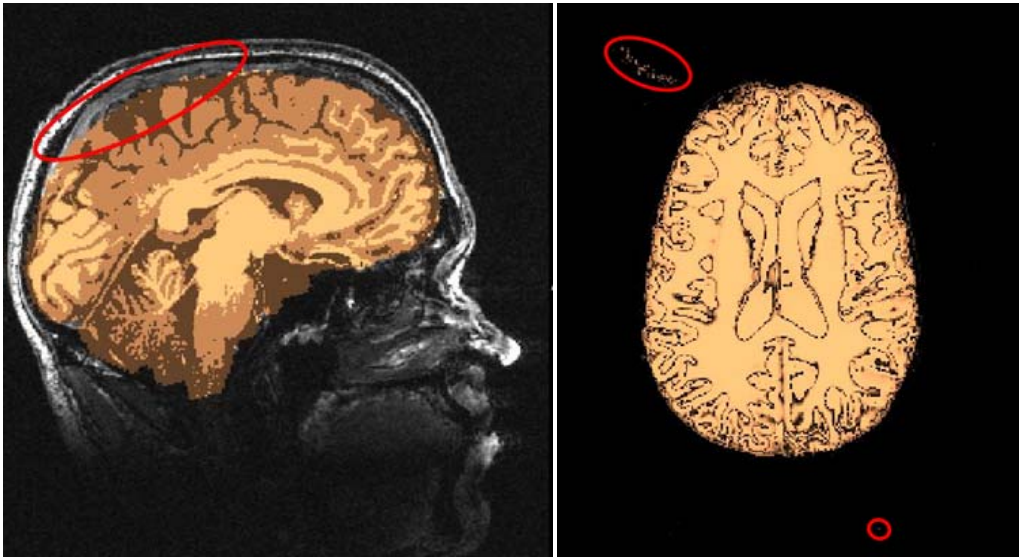


Figure 6. An example of brain extraction in FSL (left) and SPM8 (right). In FSL, the brain extraction misses part of the cortical grey matter. In SPM8, the extraction performs well, but there are a few non-brain voxels that remain (circled in red).

2.4 Tissue Segmentation

FSL's FAST is a program for segmenting three-dimensional brain images into different tissue types such as grey matter, white matter, and CSF. It uses an expectation-maximization algorithm to fit a hidden Markov random field model.^[17] The use of a hidden Markov random field model allows for inclusion of spatial information from the image by using class and intensity information of surrounding voxels. FSL automatically incorporates a bias field correction into the FAST algorithm.

Berlow's method uses iterative approach to signal intensity bias correction, brain extraction and segmentation specifically developed for MRI acquired at 7T.^[17] It includes using preprocessed images, performing segmentation with FAST and combining the results with information from R1 maps in order to get accurate segmentation. In addition to using high

resolution T₁-weighted MPRAGE, they also collect a series of images to calculate the R1 maps by solving the Bloch equation.

Segmentation in SPM8 is a voxel-based approach for tissue segmentation that uses a probabilistic framework with a mixture of Gaussians model.^[18] The method iteratively performs image registration, tissue classification, and bias correction. SPM8 uses modified versions of the International Consortium for Brain Mapping (ICBM) Tissue Probabilistic Atlases as tissue probability maps. These atlases consist of 452 T₁-weighted images classified as grey matter, white matter, and CSF. There are two options for segmentation in SPM8: Segment^[18] and New Segment.^[19] New Segment is an extension of Segment that models the whole head, not just the brain. The additional classes allow for the model to account for non-brain tissues such as air-tissue boundaries, bone, scalp, etc., thereby improving the segmentation.

2.5 Comparison of Methods on 7T Data

While the ideal dataset for comparison of segmentation algorithms is one that the “ground truth” is known, since the goal was to identify which segmentation methods work well on 7T MRI data, real 7T MRI data was used. This allows for evaluation of the segmentation algorithms on real data that has all the complications and artifacts that are typically encountered at ultra high magnetic fields.

Methods

Healthy controls (n = 13, mean age: 49 ± 9; range 24 – 65 years, 8 women and 5 men) were recruited and enrolled in an IRB approved protocol. All subjects had a comprehensive set of MR data acquisitions performed on a whole-body 7T Siemens MAGNETOM system. Scans

included high resolution 3D data sets with MPRAGE (TR = 2.3 s, TI = 1.05 s, flip angle = 6°, isotropic resolution of 0.8 mm, TA = 10.8 min) and four sets of whole brain MRI data were acquired at inversion times of 300, 900 and 2000 ms; and without inversion pulse (FOV: 192 mm x 256 mm x 192 mm, matrix: 192 x 256 x 96, TR = 2.5 s, TE = 2.3 ms, TA = 4.5 min) to calculate R1 maps by solving the Bloch equation. Examples of individual steps in the processing stream are demonstrated on a single subject.

SPM8 was used with Matlab version 2011a for all SPM analyses. FSL version 4.1 was used for all FSL analyses. The Segment routine was performed with the following parameters: Tissue probability maps: grey matter, white matter, CSF images provided by SPM8 (modified versions of the ICBM Tissue Probabilistic Atlases); Gaussians per class: two for grey matter, two for white matter, two for CSF and four for other; Affine regularisation to ICBM European brains; Warping regularisation: one; Warp frequency cutoff: 25; Bias regularisation: very light (0.0001), Bias FWHM: 60mm cutoff; sampling distance: three. The New Segment routine was performed with the same parameters as Segment with the exception of using three, four, and two Gaussians per class for the additional three classes that model non-brain tissues. To calculate tissue volumes, tissue probability images of grey matter, white matter, and CSF were created for each subject using each method.

Total tissue volumes were calculated for Berlow's, SPM8 Segment, and SPM8 New Segment methods. Since SPM8 results in an image containing probabilities of each voxel belonging to each tissue class, a threshold of 0.5 was used to avoid voxels being counted as belonging to more than one class. The FSL SIENAX tool was used to calculate vscale, a normalization factor based on skull size, in order to obtain a scaling factor to account for brain

size regardless of atrophy. Tissue volumes for FSL's FAST were not calculated because the results of the segmentation and all preceding steps were very poor, and it was obvious from the first few subjects that it does not work well for 7T imaging data without extensive modification as implemented in Berlow's method.

Results

FSL had the poorest performance of all the methods tested. The image segmentation primarily modeled the bias field variation rather than tissue classes, as the results in Figure 7 visually demonstrate, which led to extensive misclassification. FAST was additionally performed on previously bias-corrected images and still performed poorly.

SPM8 has two segmentation algorithms- Segment and New Segment. Both methods performed excellent bias field correction with a very light regularization of 0.0001. Segment failed to align 1 image properly (Figure 8). Due to the iterative and automated process of SPM8, it is difficult to make adjustments to fix problems such as this. In New Segment, all images appeared to be processed and segmented properly.

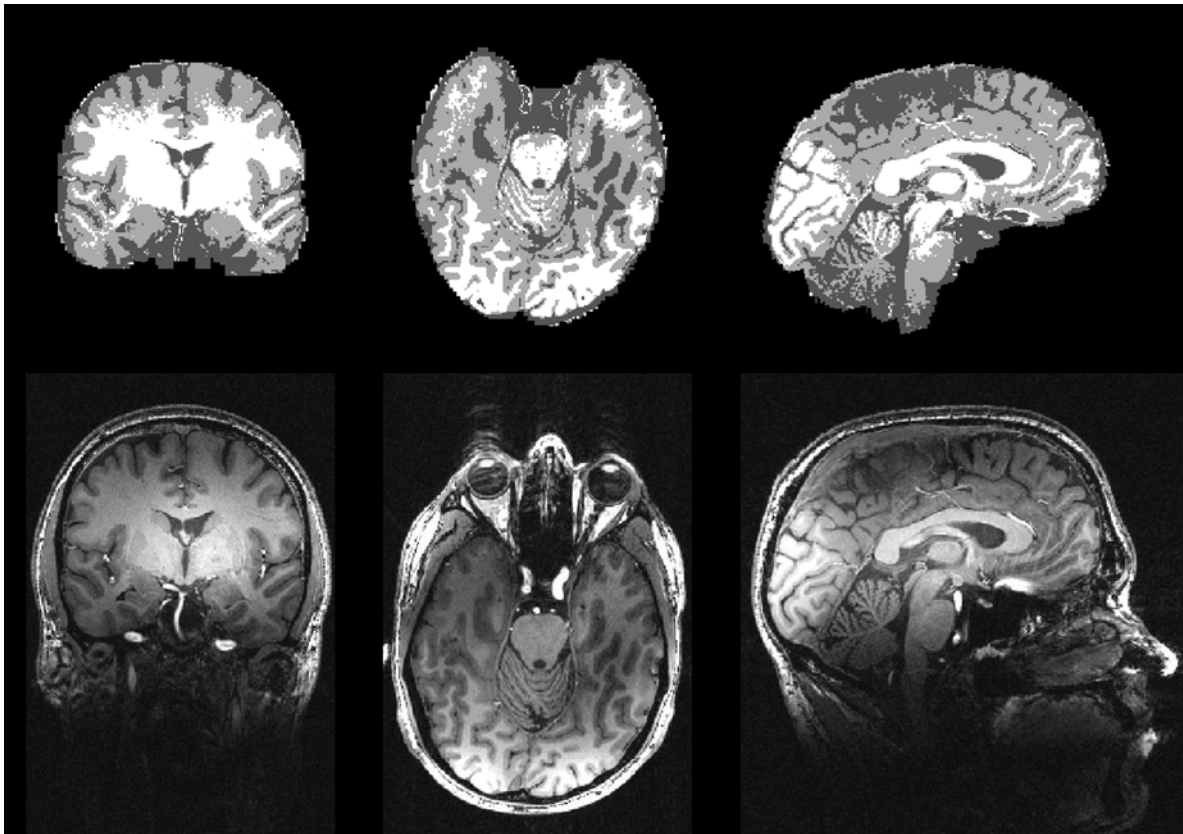


Figure 7. FSL FAST segmentation (Upper). The segmentation in FSL is far from optimal. Instead of accurately classifying the tissue into grey matter (medium grey), white matter (white), and CSF (dark grey), the model classifies variation in the bias field as tissue types, as is evident by viewing the original MR image (Lower).

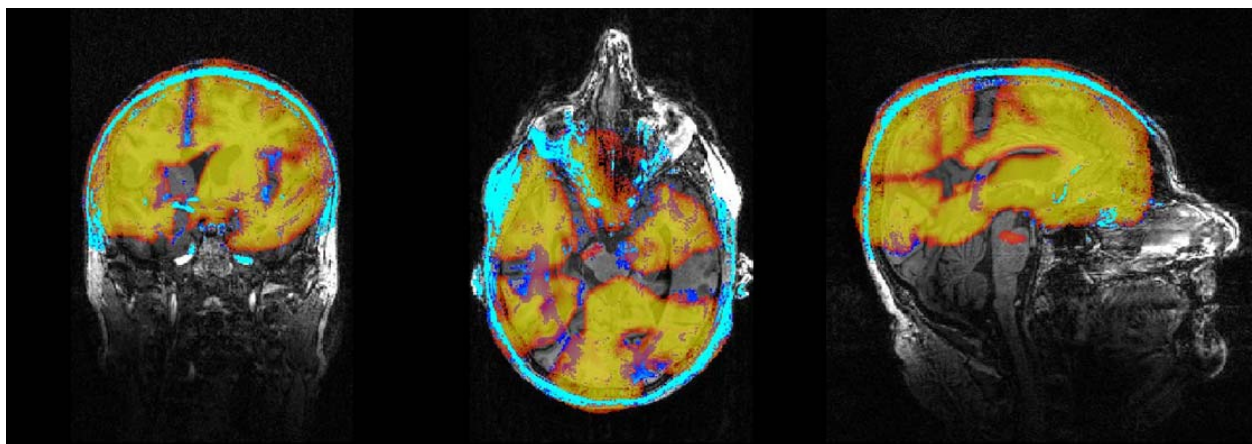


Figure 8. Improper registration of an image using SPM Segment. The grey matter segmentation image is overlaid in blue; the white matter image is overlaid in yellow/red. The New Segment method on this subject performed the segmentation unsatisfactorily.

Global GM WM CSF measures

The calculated volumes for each tissue class are summarized in Table 1. Grey and white matter measurements calculated with Segment and New Segment did not significantly differ from each other, though measurements of CSF did ($p = 0.01$). The average grey matter volume measured using Berlow's method was significantly less than Segment and New Segment measurements (Segment: $p < 0.005$, New Segment: $p = 0.03$). The white matter volume measured by Berlow's method was significantly greater than measured by the SPM8 methods (Segment: $p = 0.002$, New Segment: $p = 0.01$). CSF volumes significantly differed between Segment and both Berlow's and the New Segment methods (Berlow's method $p = 0.01$; New Segment $p = 0.01$). Berlow's method and New Segment did not significantly differ in CSF volumes.

The results of FSL's FAST are in Figure 7, showing that due to the inadequate bias field correction, FSL grossly misclassifies the majority of the grey matter, white matter, and CSF. Due to this, FSL FAST segmentation was excluded from detailed comparisons since the calculated volumes are trivial and meaningless. An overview of how the segmentation visually looked is demonstrated in Figure 9 for grey matter, Figure 10 for white matter, and Figure 11 for CSF.

Table 2. Tissue volumes measured by different segmentation methods (mean +/- standard deviation in cm^3)

	Berlow's Method	SPM8 Segment	SPM8 New Segment
GM	842 ± 101	976 ± 122	926 ± 121
WM	751 ± 68	641 ± 76	664 ± 97
CSF	356 ± 76	553 ± 272	351 ± 58

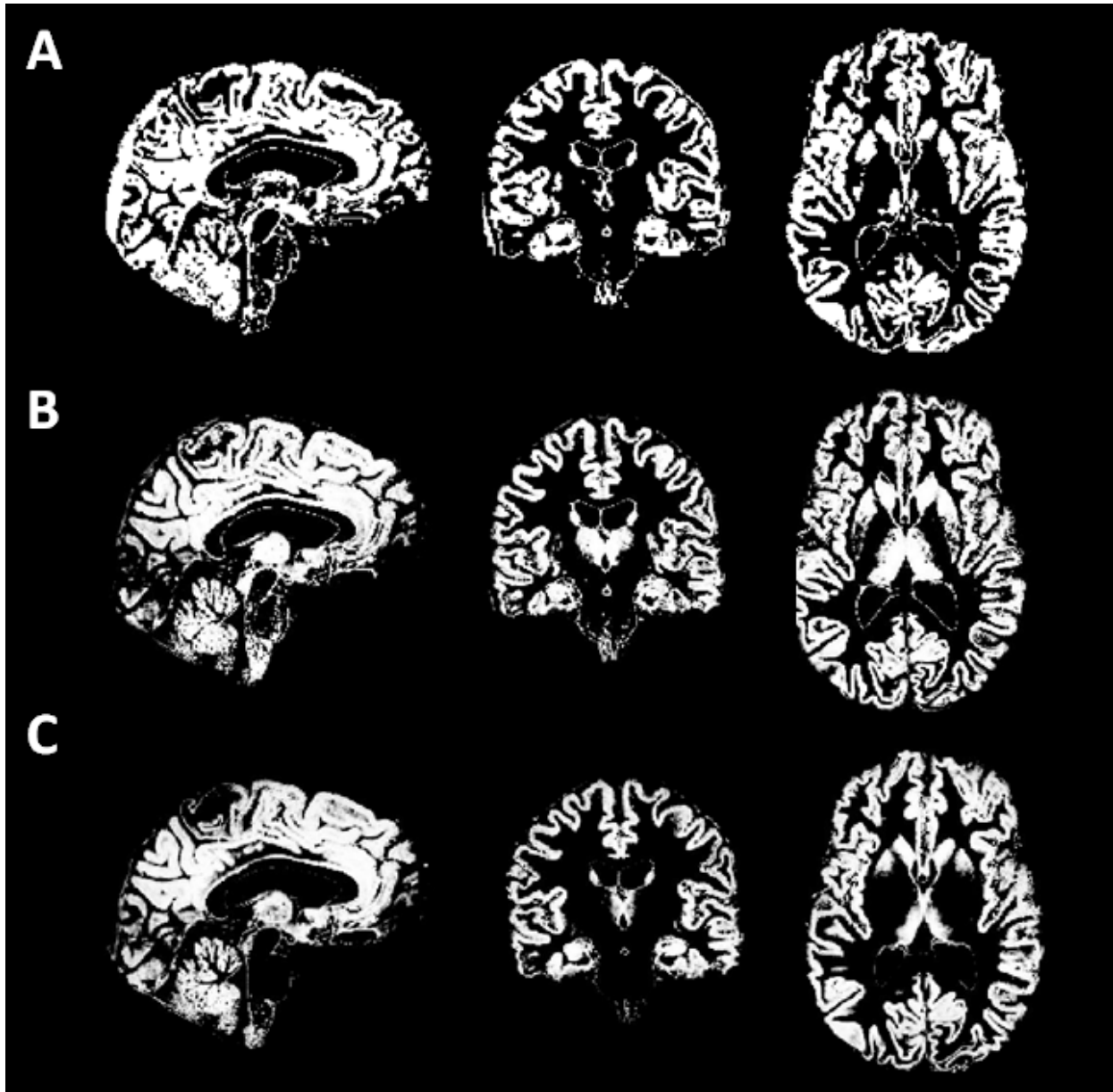


Figure 9. Overview of the grey matter segmentations evaluated. The major difference between methods appears to be in the treatment of subcortical structures. Berlow's method typically included some of the CSF labeled as grey matter at the top of the head and tended to have discontinuities in the cortical grey matter in the lower part of the brain, while New Segment and Segment did not have this tendency.

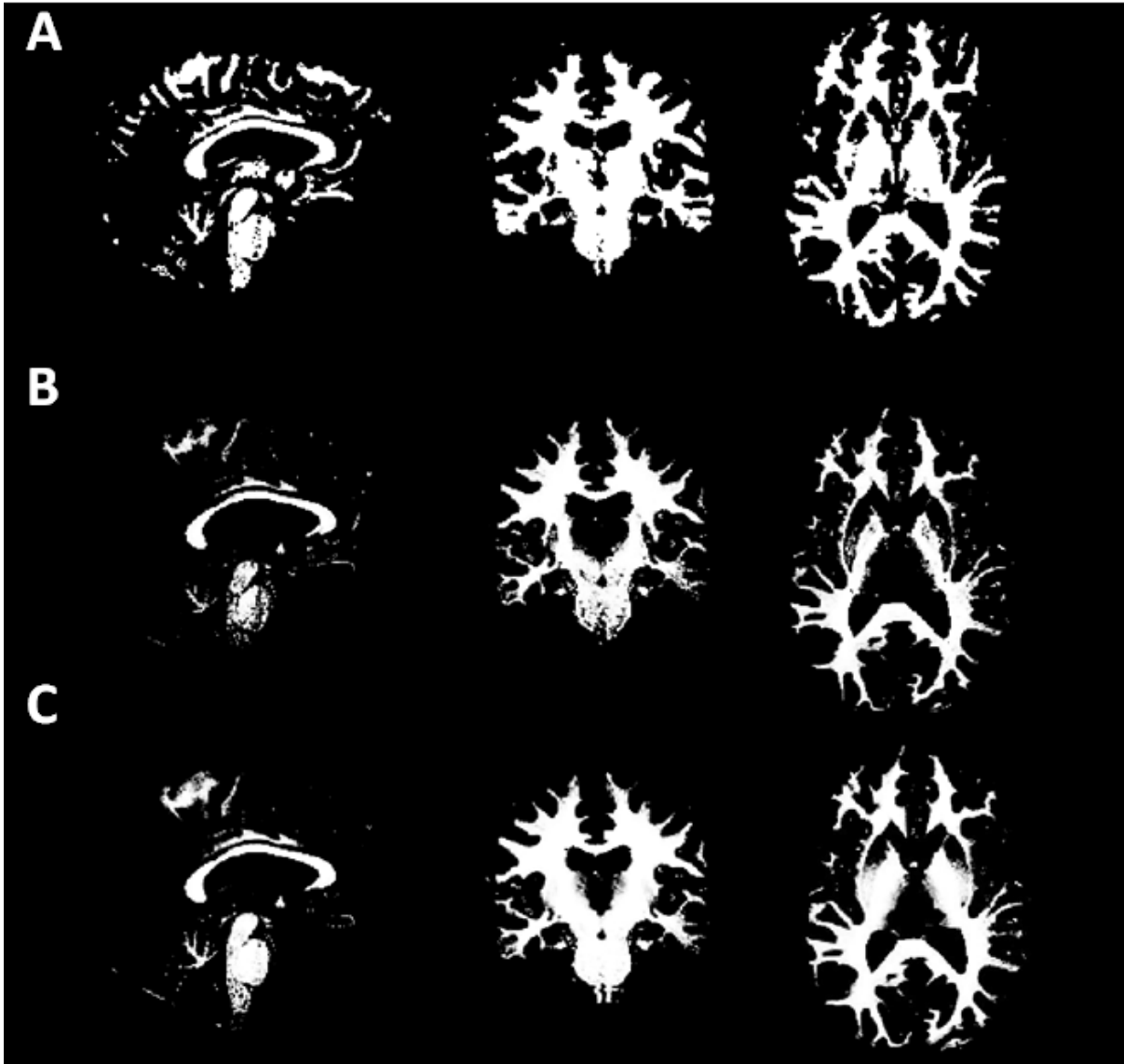


Figure 10. Overview of the white matter segmentation methods evaluated. A major difference between the SPM methods and Berlow's method appears to be in the classification of white matter on the cortical grey matter border, as is evident from the left hand column where Berlow's method shows a lot of tissue classified as white matter. The subcortical areas are again treated differently by each method.

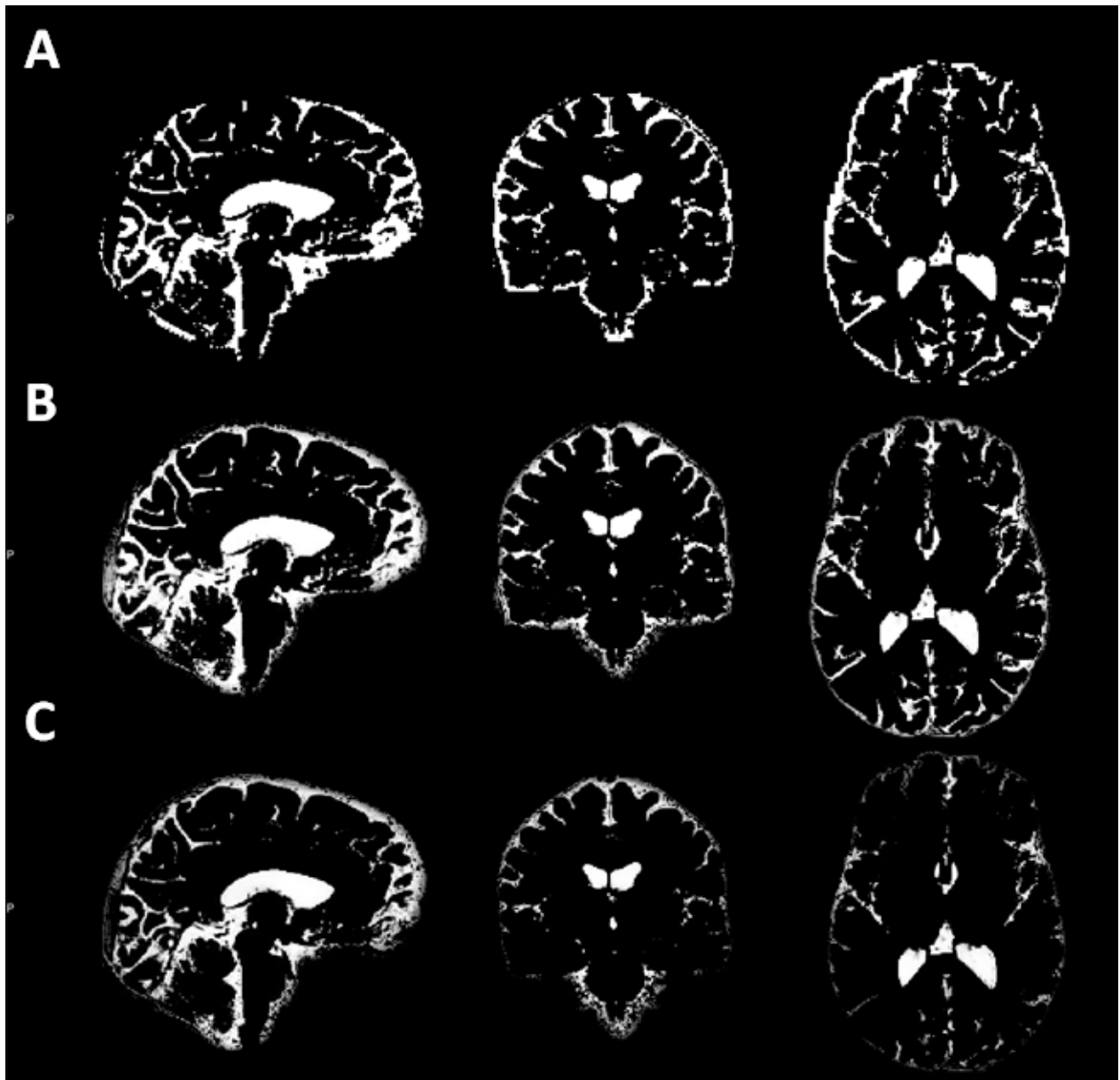
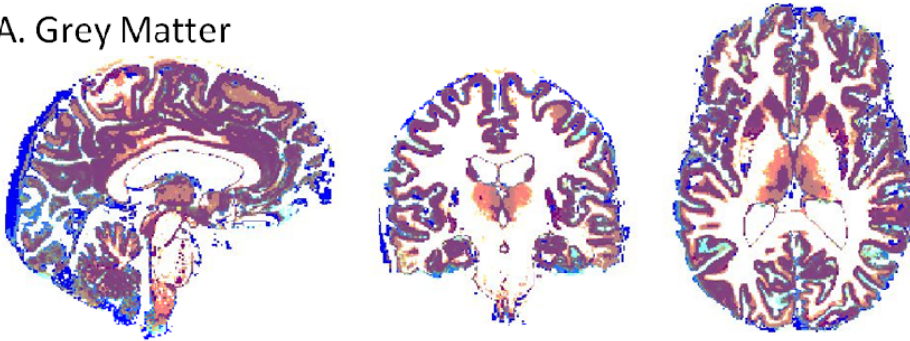
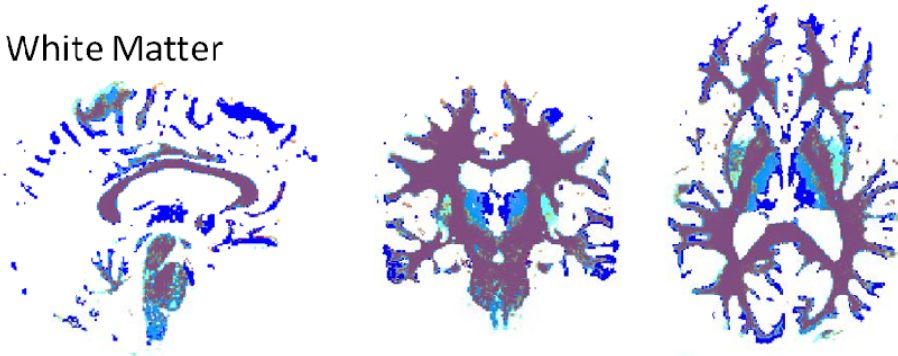


Figure 11. Overview of the CSF segmentation methods evaluated. A major difference between the methods appears to be their continuity around the brain. Segment appears to be the most continuous, while New Segment and Berlow's methods both have areas of discontinuity.

A. Grey Matter



B. White Matter



C. CSF

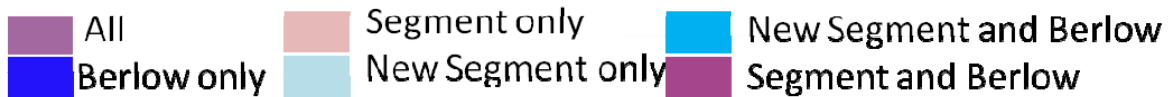
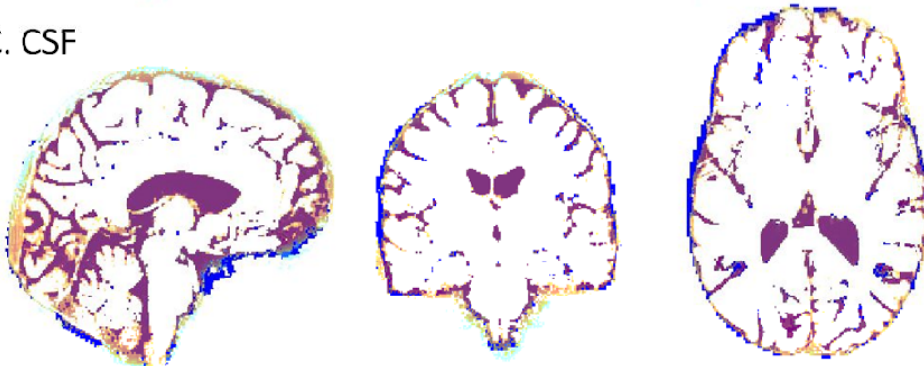


Figure 12. Color overlays of (A) grey matter, (B) white matter and (C) CSF segmentation from one subject showing the differences and similarities between the three methods used. Most of the segmentation differences arise from the classification of subcortical structures. The SPM8 Segment method classified the most subcortical tissue as grey matter, whereas the New Segment method classifies most of these structures white matter. Another difference is at the cortical grey matter - white matter border, as well as continuity of the CSF.

The measurements of CSF volume was only correlated between the Berlow method and Segment ($p = 0.02$, $r = 0.63$, Figure 13). Grey and white matter volumes were correlated between the New Segment and Segment methods (grey matter: $p = 0.01$, $r = 0.68$; white matter: $p = 0.02$, $r = 0.67$).

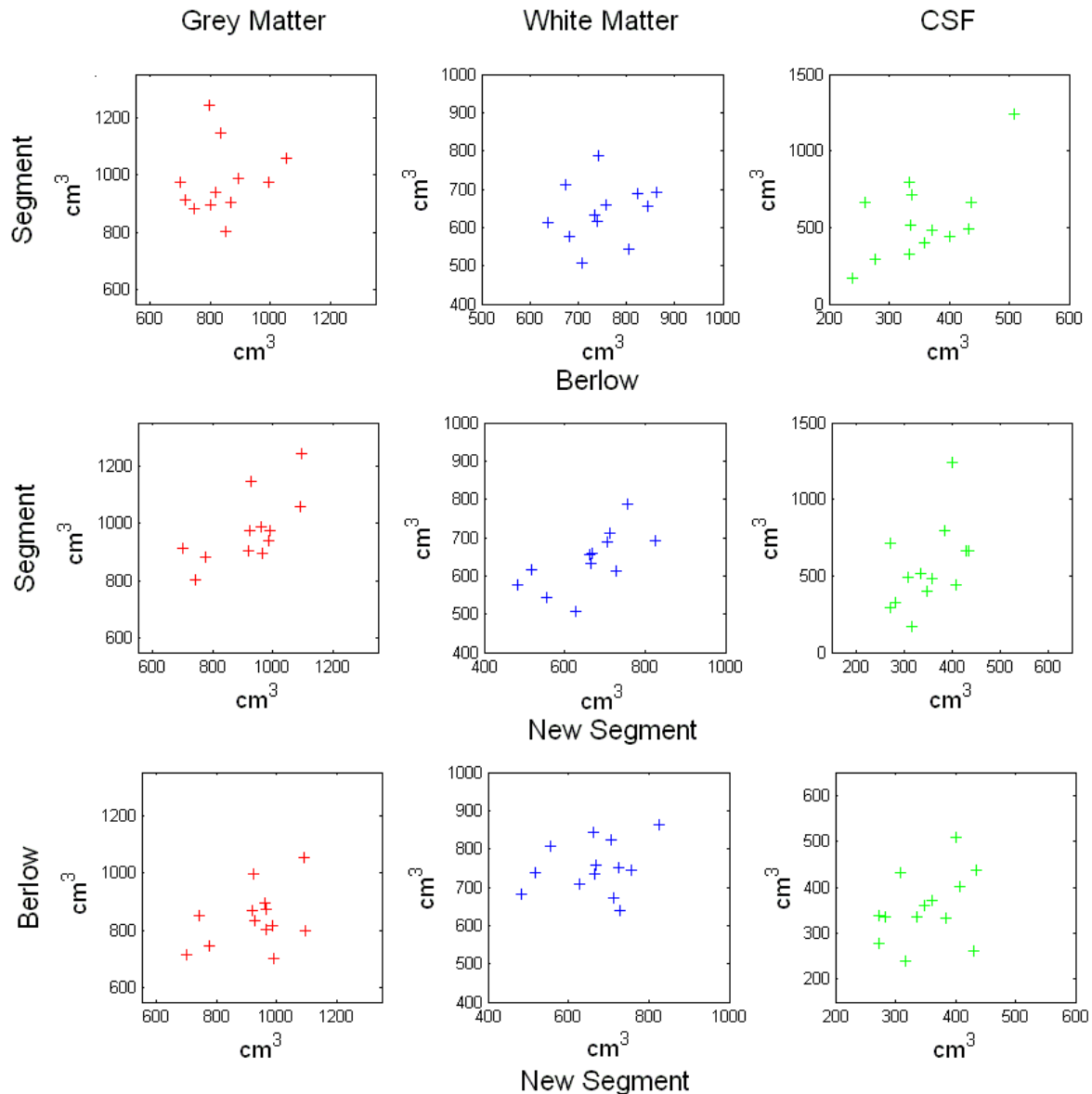


Figure 13. Scatter plots of the volumetric measurements for grey matter, white matter, and CSF using the Berlow's method, SPM8 Segment, and SMP8 New Segment. Segment and New Segment grey matter and white matter volumes have correlations with the grey and white matter volumes, while the CSF measurements from the Berlow method and Segment are also correlated.

Relationship between Age, Gender, and Volumetric Measurements.

While there was a significant relationship with age and the white and grey matter volume as measured by Berlow's method (white matter: $p = 0.05$, $r = -0.56$; grey matter: $r = -0.71$, $p = 0.007$; Figure 15), there was only one subject less than 45 years old, and this subject was 24. To evaluate if this one subject was influencing the relationship, the subject was removed. Once removed from the dataset, there were no significant relationships between brain volumes and age with any of the segmentation methods, suggesting that this data point was highly influential to the correlation. There were no significant differences found between any measures and gender.

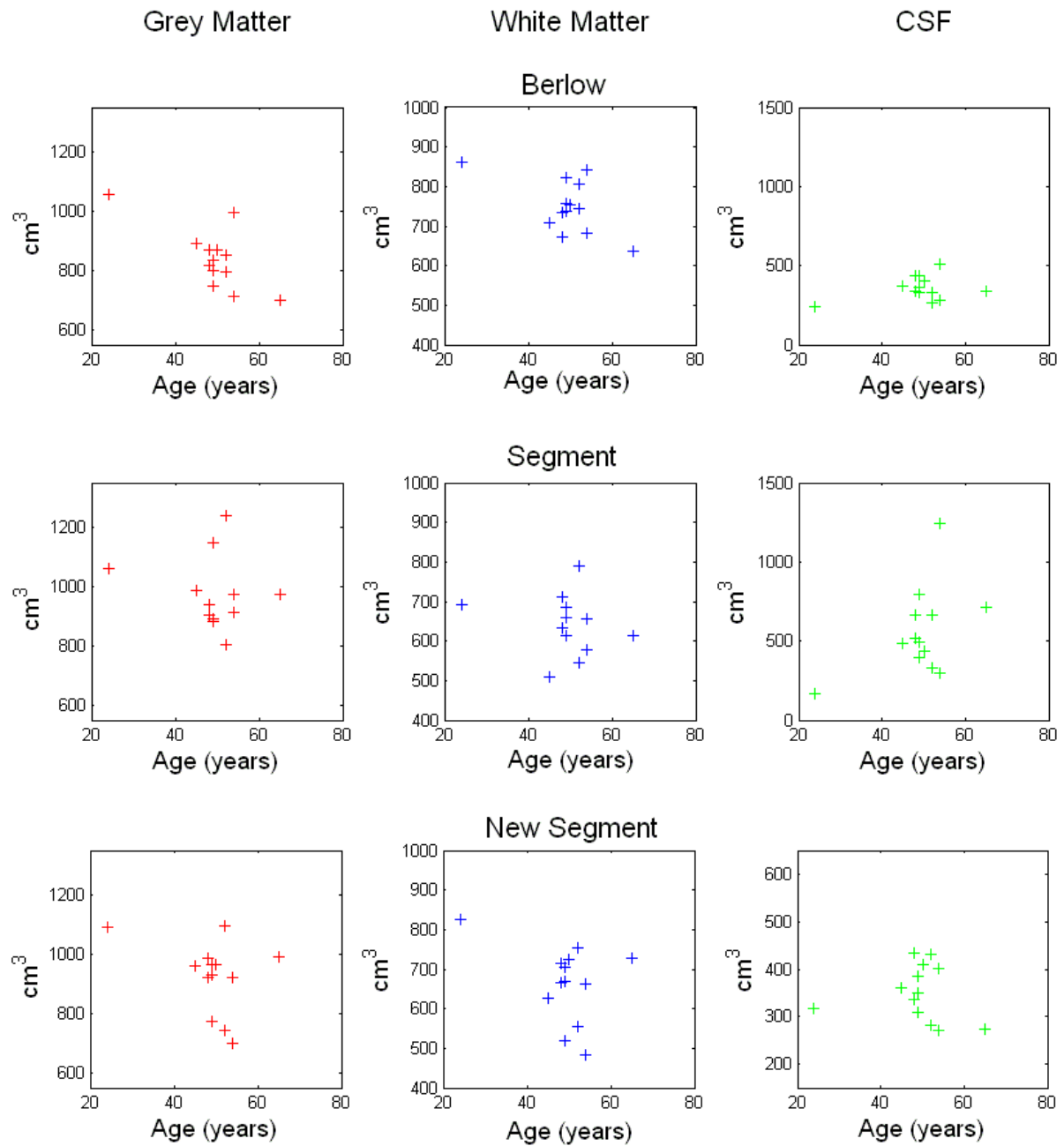


Figure 14. Scatter plots of volumetric measurements from the three methods tested versus age. Only Berlow's method had a significant correlation with grey matter volume and age, though SPM Segment and New Segment both had trends.

2.6 Discussion

Imaging at high magnetic fields shows great promise for research and potentially clinical use. The increase in signal to noise and resolution can improve the viewable detail of anatomy. While the increase in resolution is desirable to investigate anatomy with finer detail, it makes manual segmentation of images infeasible. Thus, it is desirable to have robust image segmentation tools. Due to the technical challenges with imaging at ultra high magnetic fields, applying tools developed for analysis of lower field images may not be suitable.

In this section, two common segmentation software packages- FSL and SPM8- were evaluated in order to determine their performance processing 7T MRI data. In addition, a quantitative segmentation method based on FSL tools was also evaluated. FSL's brain extraction and bias field correction were not suitable for accurately processing T1-weighted MPRAGE images collected at 7T. Even with images that were already brain extracted and bias field corrected, FSL's FAST segmentation method failed at classifying tissues correctly.

Berlow's method was efficient at correcting the bias field inhomogeneities, extracting the brain tissue, and performing segmentation. This method did miss some areas of grey matter that were thin and close to the scalp, as well as some grey matter in the cerebellum. One shortcoming of this method is that it is not available as an automated work stream yet and involved incorporating a lot of information in addition to an MPRAGE image, including calculation of R1 maps.

SPM8 handled the technical problems with 7T data well. The iterative process of estimating the bias field, registering, and performing the tissue segmentation based on priors effectively adjusted the bias field inhomogeneities in the images.

One shortcoming of SPM8 in comparison to FSL is that since it is built in Matlab and designed to be used with a GUI, it is inefficient since it does not take advantage of parallel programming and has some graphics which do not add to the usability but use a lot of computing resources. Some users have developed a work around for this limitation with NiPype.^[16] While this is extremely useful in improving the SPM8 workflow, it can be difficult to determine how to change the default settings or what the default settings are.

SPM's Segment and New Segment did not significantly differ in the volumes of white matter or grey matter, but did differ in CSF volumes. Berlow's method significantly differed with on all measures compared from other methods. The cause of this difference appears to be how each method handles the classification of the subcortical structures. Even if volumetric measurements differ, which is not surprising given the differences in the methods, they might be expected to correlate to each other. However, the only measures that had a significant correlations were grey and white matter measured by Segment and New Segment, and CSF measured by Berlow's method and SPM8 Segment. This is surprising because all methods appeared to perform the tissue segmentation well.

Klauschen et al. compared the ability of the algorithms in FSL, SPM5, and FreeSurfer to segment MRI images from the BrainWeb MRI database into white matter and grey matter.^[20] All methods had a deviation between 1% and 11% from the reference values of white and grey matter. In terms of performance, FSL and SPM5 had similar volumetric accuracy, both of which outperformed FreeSurfer. SPM5 was found to have the best sensitivity. They also tested the robustness of image quality changes, and showed that FSL had the highest stability for white matter and FreeSurfer had the highest stability for grey matter.

Tsang et al. also compared a previous release of SPM, SPM5 to FSL version 4. In SPM5, only the Segment segmentation protocol was available. They compared the results of brain segmentation using brain phantom MRI images from the BrainWeb MRI database, a real dataset, and an expert-segmented dataset from Internet Brain Segmentation Repository (IBSR) provided by Massachusetts General Hospital.^[21] They found that SPM5 consistently performed slightly better than FSL, but the results were not statistically significant.

While previous studies have evaluated the SPM Segment in comparison to FSL's FAST and found SPM to perform better, these studies were performed on 3T images. To our knowledge, no one has compared the performance of automated segmentation software on 7T MR images. Here, two SPM segmentation methods, FSL's FAST method, and an extension of FSL's method were evaluated. The two SPM segmentation methods performed similar to each other whereas FSL performed poorly on the 7T data. Using a method involving additional iterative processing and information from quantitative R1 maps, Berlow et al. developed a method for segmenting 7T images using FSL tools including FAST.^[17] This method performed well on processing and segmenting the 7T MR images. All methods that performed satisfactorily varied in their volume estimations. This is due to differences in identifying voxels along the white matter - grey matter border, classifying the tissue of subcortical structures, and could also be due to the inclusion of background noise or exclusion of parts of the brain. Without images where the "ground truth" is known, it is difficult to identify which of these methods performed the best.

References

- 1) P.C. Lauterbur. Image formation by induced local interactions: examples employing nuclear magnetic resonance *Nature* **1973**, *242*, 190-191.
- 2) E.R. Andrew. N.m.r. Imaging of Intact Biological Systems *Philosophical Transactions of the Royal Society of London. Series B, Biological Sciences* **1980**, *289*, 471-481.
- 3) R. deGraaf. *In Vivo NMR Spectroscopy Principles and Techniques*; John Wiley and Sons: West Sussex, 1998.
- 4) J. P. Hornak. *The Basics of MRI*. Interactive Learning Software, Henrietta, New York. **2004**. <http://www.cis.rit.edu/htbooks/mri/>
- 5) P. Mansfield. Imaging by Nuclear Magnetic Resonance *J. Phys. E: Sci. Instrum* **1988**, *21*, 18-30
- 6) C.M.J. de Bazelaire, G.D. Duhamel, N.M.Rofsky, D.C. Alsop. MR Imaging Relaxation Times of Abdominal and Pelvic Tissues Measured in Vivo at 3.0T: Preliminary Results *Radiology* **2004**, *230*, 652-659
- 7) G.J. Stanisz, E.E. Odobina, J. Pun, M. Escaravage, S.J. Graham, M.J. Bronskill, R.M. Henkelman. T1, T2 relaxation and magnetization transfer in tissue at 3T. *Magnetic Resonance in Medicine* **2005**, *54*, 507-512.
- 8) P. Schmitt, M.A. Griswold, P. Jakob, M. Kotas, V. Gulani, M Flentje, A Haase, Inversion recovery TrueFISP: quantification of T(1), T(2), and spin density. *Magnetic Resonance in Medicine* **2004**, *51*, 661-667.
- 9) J.T. Vaughan, M Garwood, CM Collins, W Liu, L DelaBarre, G Adriany, P Andersen, H Merkle, R Goebel, MB Smith, K Ugurbil. 7T vs. 4T: RF power, homogeneity, and signal-to-noise comparison in head images. *Magn Reson Med.* **2001**, *46*(1):24-30.
- 10) F. Lüsebrink, A. Wollrab, O. Speck. Cortical thickness determination of the human brain using high resolution 3T and 7T MRI data. *NeuroImage.* **2013**, *70*:122-31.
- 11) H. Suzuki and J. Toriwaki. Automatic segmentation of head MRI images by knowledge guided thresholding. *Computerized medical imaging and graphics.* **1991**, *15*(4):233-240.
- 12) M.C. Clark, L.O. Hall, D.B. Goldgof, L.P. Clarke, R.P. Velthuizen, and M.S.Silbiger. MRI segmentation using fuzzy clustering techniques. *Engineering in Medicine and Biology Magazine, IEEE,* **2002**, *13*(5):730-742.
- 13) Z.Y. Shan, G.H. Yue, and J.Z. Liu. Automated histogram-based brain segmentation in T1-weighted three-dimensional magnetic resonance head images. *NeuroImage* **2002**, *17*(3):1587-1598.
- 14) Y. Wang, T. Adali, S.Y. Kung, and Z. Szabo. Quantification and segmentation of brain tissues from MR images: A probabilistic neural network approach. *Image Processing, IEEE Transactions on,* **2002**, *7*(8):1165-1181.

- 15) Y. Zhang, M. Brady, and S. Smith. Segmentation of brain mr images through a hidden markov random field model and the expectation maximization algorithm. *Medical Imaging, IEEE Transactions on*, **2001**, 20(1):45-57.
- 16) Gorgolewski K, Burns CD, Madison C, Clark D, Halchenko YO, Waskom ML, Ghosh SS. (2011). Nipype: a flexible, lightweight and extensible neuroimaging data processing framework in Python. *Front. Neuroinform.* 5:13.
- 17) Y. Berlow, M.K. Sammi, A.H. Selzer, D. Bourdette, W.D. Rooney. Quantitative Volumetrics of Multiple Sclerosis Brain from 7T MRI. *Proc. Int. Soc. Magn. Reson. Med.* **2013**. 21, 4692.
- 18) J. Ashburner and K.J. Friston. Unified segmentation. *NeuroImage*, **2005**, 26(3):839-851.
- 19) J. Ashburner. SPM: A history. *NeuroImage* **2012**, 62(2):791–800.
- 20) F. Klauschen, A. Goldman, V. Barra, A. Meyer-Lindenberg, and A. Lundervold. Evaluation of automated brain MR image segmentation and volumetry methods. *Human brain mapping*, **2009**, 30(4):1310-1327.
- 21) O. Tsang, A. Gholipour, N. Kehtarnavaz, K. Gopinath, R. Briggs, and I. Panahi. Comparison of tissue segmentation algorithms in Neuroimage analysis software tools. 30th Annual International IEEE EMBS Conference. Vancouver, British Columbia, Canada, August 20-24, **2008**